Mem. S.A.It. Suppl. Vol. 24, 111

Memorie della
Supplementi

Oxygen spectral line synthesis: 3D non-LTE with CO5BOLD hydrodynamical model atmospheres

D. Prakapavičius[1], M. Steffen[2,6], A. Kučinskas[1,3], H.-G. Ludwig[4], B. Freytag[5], E. Caffau[4,6], R. Cayrel[6]

[1] Vilnius University Institute of Theoretical Physics and Astronomy, A. Goštauto 12, Vilnius LT-01108, Lithuania
[2] Leibniz-Institut für Astrophysik Potsdam, An der Sternwarte 16, D-14482, Potsdam, Germany
[3] Vilnius University Astronomical Observatory, M. K. Čiurlionio 29, Vilnius LT-03100, Lithuania
[4] ZAH Landessternwarte Königstuhl, D-69117 Heidelberg, Germany
[5] Centre de Recherche Astrophysique de Lyon, UMR 5574, CNRS, Université de Lyon, École Normale Supérieure de Lyon, 46 Allée d'Italie, F-69364 Lyon Cedex 07, France
[6] GEPI, Observatoire de Paris, CNRS, UMR 8111, 61 Av. de l'Observatoire, 75014 Paris, France

Abstract. In this work we present first results of our current project aimed at combining the 3D hydrodynamical stellar atmosphere approach with non-LTE (NLTE) spectral line synthesis for a number of key chemical species. We carried out a full 3D-NLTE spectrum synthesis of the oxygen IR 777 nm triplet, using a modified and improved version of our NLTE3D package to calculate departure coefficients for the atomic levels of oxygen in a CO5BOLD 3D hydrodynamical solar model atmosphere. Spectral line synthesis was subsequently performed with the Linfor3D code. In agreement with previous studies, we find that the lines of the oxygen triplet produce deeper cores under NLTE conditions, due to the diminished line source function in the line forming region. This means that the solar oxygen IR 777 nm lines should be stronger in NLTE, leading to negative 3D NLTE–LTE abundance corrections. Qualitatively this result would support previous claims for a relatively low solar oxygen abundance. Finally, we outline several further steps that need to be taken in order to improve the physical realism and numerical accuracy of our current 3D-NLTE calculations.

1. Introduction

Photospheric abundances of chemical elements derived from stellar spectra are important means for testing and constraining models of the formation and evolution of the Galaxy and its various stellar populations. The reliability of the derived chemical abundances is limited, apart from the quality of the observational data, by the realism of the ingredients used in the abundance analysis: atomic data that describe the spectral lines themselves, stellar model atmospheres, and the allowance of possible departures from local thermodynamic equilibrium (LTE).

During the recent years, reliable spectral line data has been measured and/or computed for a large number of astrophysically

relevant spectral lines, and departures from LTE are currently accounted for with an increasingly more realistic treatment of collisional processes. However, the stellar model atmospheres that are commonly used for the abundance analysis are based on a number of critical simplifications: they are typically constructed in one-dimensional (1D) geometry - plane-parallel or spherically-symmetric - and are subject to hydrostatic and radiative-convective equilibrium (see, e.g., Castelli & Kurucz 2004; Brott & Hauschildt 2005; Gustafsson et al. 2008). Even though the input microphysics (opacities, equation of state) of these models is sufficiently realistic, the convective energy transport, one of the main processes shaping the physical structure of the photosphere, is treated in the approximation of the mixing-length theory (Böhm-Vitense 1958) or its derivatives (Canuto & Mazzitelli 1991).

In this respect, three-dimensional (3D) hydrodynamical stellar model atmospheres are much more realistic, as they are able to account for convection based on first principles without the need of free parameters (see Nordlund 1982; Stein & Nordlund 1998; Asplund et al. 2000; Freytag et al. 2002; Wedemeyer et al. 2004). Moreover, this type of model atmospheres naturally allows for the emergence of a surface granulation pattern, horizontal inhomogeneities and wave activity, all being unique properties of 3D hydrodynamical model atmospheres. It has been found that the interplay of these physical processes significantly alters spectral line formation, which may lead to substantial differences in the abundances derived with 3D and 1D model atmospheres, respectively (Collet et al. 2007; Dobrovolskas et al. 2010; Ivanauskas et al. 2010; Kučinskas et al. 2013; Dobrovolskas et al. 2013). These findings conspicuously indicate that the 3D photospheric structure and dynamics has a significant impact on the spectral line formation, and should be properly taken into account in the chemical abundance analysis.

Besides the application of realistic stellar model atmospheres, an adequate treatment of non-LTE (NLTE) processes can be also very important for deriving reliable chemical abundances. In the optically thin line-forming regions, the absorbing particles experience a radiation field that is of non-local origin since it forms deeper in the photosphere. Consequently, radiation field in the line-forming region may exhibit significant deviations from the local Planck function. Radiation of non-local origin can distort the collisional ionization balance given by the Saha equation, and drive the population numbers of the upper and lower atomic levels of the given transition away from the Boltzmann distribution that is valid in LTE (for a thorough discussion of these effects see, e.g. Bruls et al. 1992). Departures from LTE modify both the strength and shape of the spectral lines, and therefore can significantly alter spectroscopically derived chemical abundances, in particular at low metallicities (e.g., Thévenin & Idiart 1999).

Given the significance of NLTE effects and the magnitude of the LTE 3D-1D abundance corrections (especially in the metal-poor stars), it is obvious that the two factors should be simultaneously taken into account in order to derive reliable abundance estimates. However, the joint 3D-NLTE approach has only been applied in a few selected cases so far (Asplund et al. 2004; Shchukina et al. 2005; Cayrel et al. 2007; Pereira et al. 2009; Sbordone et al. 2010; Steffen et al. 2012), therefore a systematic application of this admittedly very demanding methodology to, e.g., the investigation of stellar populations, is yet to come.

Driven by the need to combine modern 3D stellar model atmospheres and non-LTE spectral line synthesis, we have recently started a project to make this methodology available for a wider range of chemical elements to be studied with 3D hydrodynamical CO^{5}BOLD stellar model atmospheres. Oxygen is a particularly interesting element to investigate using the full 3D NLTE approach: it is the most abundant chemical element besides hydrogen and helium, and its photospheric abundance is widely used to trace the formation and chemical evolution of various Galactic populations. It is well known that the O I IR triplet (λ = 777 nm) experiences significant departures from the LTE (Kiselman 1993; Fabbian et al. 2009, and ref-

erences therein). Due to its high ionization potential, oxygen does not experience significant overionization in late-type stars, so that NLTE effects are mainly limited to deviations from the thermal excitation equilibrium. These physical aspects limit the range of possible NLTE effects in the case of oxygen and therefore make it a good test case for the full 3D-NLTE approach with CO^{5}BOLD model atmospheres.

2. Methodology

2.1. Model atmospheres

The 3D hydrodynamical solar model atmosphere used in this work was computed with the CO^{5}BOLD code (Freytag et al. 2012). The CO^{5}BOLD code solves time-dependent equations of compressible hydrodynamics and radiation transfer on a 3D Cartesian grid. Computed in the "box-in-a-star" setup (for details see, e.g., Freytag et al. 2012), our solar model atmosphere was allowed to evolve hydrodynamically for several convective turnover times (see Ludwig & Kučinskas 2012, Appendix A, for a definition of different time scales). This particular CO^{5}BOLD simulation was also used in the studies of Caffau et al. (2008) and Beeck et al. (2012), to which we refer the reader for a more detailed description of the input microphysics and physical properties of the model itself.

A representative sub-sample of twenty 3D model snapshots (i.e. model structures calculated at different instants in time) was chosen out of the relaxed part of the 3D model run in order to produce a statistically representative and uncorrelated snapshot selection. More specifically, snapshots in this sub-sample were chosen in such a way that the average emerging radiation flux and its standard deviation would match the corresponding values of the entire 3D model run. Similar requirements were applied in the case of the horizontally averaged vertical mass flux at characteristic optical depths. The final selection of the 3D model snapshots obtained according to these criteria was subsequently used in the evaluation of NLTE effects (Sect. 2.2) and, later, in the spectral synthesis calculations of the O I IR triplet (Sect. 2.3).

The original model snapshots had 140 grid points in each horizontal direction and 150 grid points on the vertical axis, corresponding to a spatial coverage of $5.6 \times 5.6 \times 2.27$ Mm. The vertical grid of the model spanned the optical depth range of $-6.7 < \log \tau_{\rm Ross} < 5.5$, which is sufficient to cover the depths where the O I IR triplet lines form. For the calculation of departure coefficients and spectral line synthesis, a coarser 3D model atmosphere was constructed by choosing every third grid point horizontally, thereby reducing horizontal resolution of the model to 47×47 grid points. We have verified that differences in the spectral synthesis results obtained with the full and reduced model atmospheres, respectively, were negligible.

2.2. NLTE calculations

Departures from LTE in the line formation computations are quantified via three-dimensional sets of departure coefficients[1] which in our study were computed with the NLTE3D code (see Cayrel et al. 2007; Steffen et al. 2012). We have recently made numerous improvements and generalizations to the code in order to adapt it for a wider variety of model atoms and astrophysical tasks. More specifically, we included IONDIS/OPALAM routines, originally part of the Kiel stellar atmosphere package. These routines provide partition functions for a variety of chemical species and are also used for the computation of LTE population numbers and continuous opacities at the wavelengths of the line transitions in a given model atom. Since these routines are also used in the spectrum synthesis code Linfor3D (Sect. 2.3), this also contributes towards the self-consistency between the NLTE3D and Linfor3D packages.

During the first step, the NLTE3D code computes photo-ionization and collisional rates, where the upward and downward col-

[1] The departure coefficient for atomic level $i = 1 \ldots i_{\rm max}$ is defined as $b_i = N_{i,\,\rm NLTE}/N_{i,\,\rm LTE}$, where N_i is the level population for the respective case.

lisional rates are treated in detailed balance and, hence, only the upward rates need to be computed explicitly. These rates are kept constant throughout all further computations. After this step, radiation transfer calculations are done for each of the considered line transitions, $\ell = 1 \ldots \ell_{\max}$, to compute the mean line intensity $\overline{J_\ell}(x, y, z)$ at all grid points, where J refers to the angle-averaged intensity, and overbar indicates averaging over the line profile. Typically, we use 16 inclined plus the vertical direction for angular averaging, and 37 frequencies to resolve the line profile. Then, the photo-excitation rates are computed using $\overline{J_\ell}$, and all rates at each grid point of the 3D model snapshot are passed to the statistical equilibrium routines that compute NLTE population densities according to the prescriptions given in Mihalas (1970). Given $\overline{J_\ell}$, a set of linear equations needs to be solved for the unknown departure coefficients $b_i, i = 1 \ldots i_{\max}$, which is done using standard linear algebra routines, independently for each 3D model grid cell.

Once the new iteration of NLTE population numbers is completed, the NLTE line opacities are updated and the next iteration is started to compute line radiation transfer in order to obtain updated photo excitation rates. This cycle is repeated via the ordinary Λ-iteration scheme until the relative change in the selected NLTE line equivalent widths (EWs) becomes less than 10^{-3} per iteration (see also Sect. 3.2).

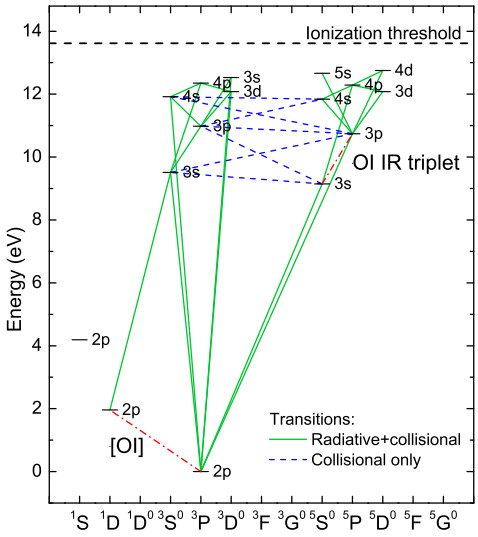

Fig. 1. Oxygen model atom used in this work. Radiatively allowed transitions are marked by solid (green) lines, while radiatively forbidden transitions that were treated only via electron-impact excitation are marked by dashed (blue) lines. The forbidden [O I] line and the O I IR triplet are marked by dash-dotted (red) lines. Collisional and radiative bound-free transitions were taken into account for each level.

2.2.1. The oxygen model atom

The Grotrian diagram of the oxygen model atom used in our study is shown in Fig. 1. The model atom consists of $i_{\max} = 16$ levels, connected by 16 bound-free and $\ell_{\max} = 31$ bound-bound transitions. Atomic data that describe the levels (energies, statistical weights) and radiative transitions (Einstein coefficients) were taken from the NIST database. Photoionization cross-sections for the radiative bound-free transitions were adopted from the Topbase of the Opacity Project (Cunto et al. 1993, and further updates).

Excitation and ionization due to collisions with neutral hydrogen atoms was treated via the Drawin (1969) formula in the formulation of Lambert (1993). In the present work, we set $S_{\rm H}$, a parameter that scales the hydrogen collision rates, to 1.0. Collisional ionization by electrons was treated using the classical prescription of Seaton (1962). Rate coefficients for the excitation by inelastic electron collisions were taken from the work of Barklem (2007), allowing us to include the collisional transitions between the triplet and quintet systems. Finally, we include a resonant charge transfer reaction $O^0 + H^+ \rightleftharpoons O^+ + H^0$ for the ground level of oxygen, in the prescription by Arnaud & Rothenflug (1985). The latter process is very efficient in late-type stars and therefore ensures that the ground level of O II is in LTE with respect to the ground level of O I.

For the computation of the photo-ionizing radiation flux, opacity distribution functions from Castelli & Kurucz (2004) were used, while the continuous opacity was calculated with the IONDIS/OPALAM routines. Background opacities stemming from the bound-bound transitions of elements other than oxygen are not yet included in the current version of the NLTE3D code. Tests have shown, however, that they are not important in the case of the oxygen model atom used in this study.

In the statistical equilibrium calculations, we treated the O I ground level ($2p^3P$) and the upper level of the O I IR triplet ($3p^5P$) as singlets, while, when performing spectrum synthesis calculations, we have taken the fine-splitting into account, assuming that the departure coefficients are identical for all sub-levels: due to their close energetic values, they should be efficiently thermalized and thus experience identical sensitivity to NLTE effects.

2.3. Spectral synthesis calculations

Spectral synthesis calculations of the O I IR triplet lines were done with `Linfor3D`[2]. Firstly, `Linfor3D` calculates the LTE line source function, $S_{\rm LTE}(\nu) = B_\nu$ (Planck's black body function) and line opacity, $\kappa_{\rm LTE}(\nu)$ for any given line transition. Whenever NLTE spectrum synthesis is requested, both the line source function and the line opacity are modified according to:

$$\frac{S_{\rm NLTE}(\nu)}{S_{\rm LTE}(\nu)} = \frac{\exp(\frac{h\nu}{kT}) - 1}{(b_{\rm low}/b_{\rm up})\,\exp(\frac{h\nu}{kT}) - 1}\,, \qquad (1)$$

and

$$\frac{\kappa_{\rm NLTE}(\nu)}{\kappa_{\rm LTE}(\nu)} = b_{\rm low}\,\frac{\exp(\frac{h\nu}{kT}) - (b_{\rm up}/b_{\rm low})}{\exp(\frac{h\nu}{kT}) - 1}\,, \qquad (2)$$

where $b_{\rm low}$ and $b_{\rm up}$ are the departure coefficients of the lower and upper level of the transition, respectively. Once the line source function and line opacity are computed either in LTE or NLTE, the radiation transfer is calculated along 16 inclined plus the vertical direction, taking into account the differential Doppler shifts along each line-of sight. This procedure is repeated for every of the twenty 3D model snapshots. Finally, the resulting spectral lines synthesized along each of the different directions are combined into a single spectral line profile by spatial, temporal, and angular averaging.

[2] http://www.aip.de/~mst/Linfor3D/linfor.pdf

3. Results

3.1. Synthetic O I IR triplet spectra

We have conducted NLTE and LTE spectrum synthesis calculations of the O I IR triplet lines using a 3D solar model atmosphere computed with the `CO5BOLD` code. Fig. 2 shows the obtained synthetic NLTE and LTE O I IR triplet spectrum (identical oxygen abundances were used in the LTE and NLTE computations). It can be immediately seen that both shape and strength of the O I IR triplet lines is sensitive to NLTE effects: while the line wings are very similar in both cases, deeper line core is present in NLTE. Hence, in accordance with the previous studies, NLTE effects lead to higher equivalent widths of the O I IR triplet lines and to negative 3D NLTE–LTE abundance corrections. Such behavior is qualitatively very similar to that reported by Asplund et al. (2004) or Pereira et al. (2009), which was found to be one of the major factors leading to a lower solar oxygen abundance.

The nature of the NLTE spectral line formation can be investigated by examining the dependence of NLTE effects on the continuum intensity across the stellar surface, where high and low continuum intensity represents granular and intergranular regions, respectively. Fig. 3 shows the distribution of the NLTE to LTE ratios of local EWs computed from the vertical ray (disk-center intensity) and plotted versus the local relative continuum intensity. While the plot reveals significant differences with respect to the results obtained by Asplund et al. (2004, Fig. 4), who found diminished NLTE EWs in some (tough not all) intergranular lanes, our results show a quite good qualitative agreement with the computations of Kiselman (1993, Fig. 8) (note, however, that the adopted $S_{\rm H}$ values were different in all three investigations). Our results indi-

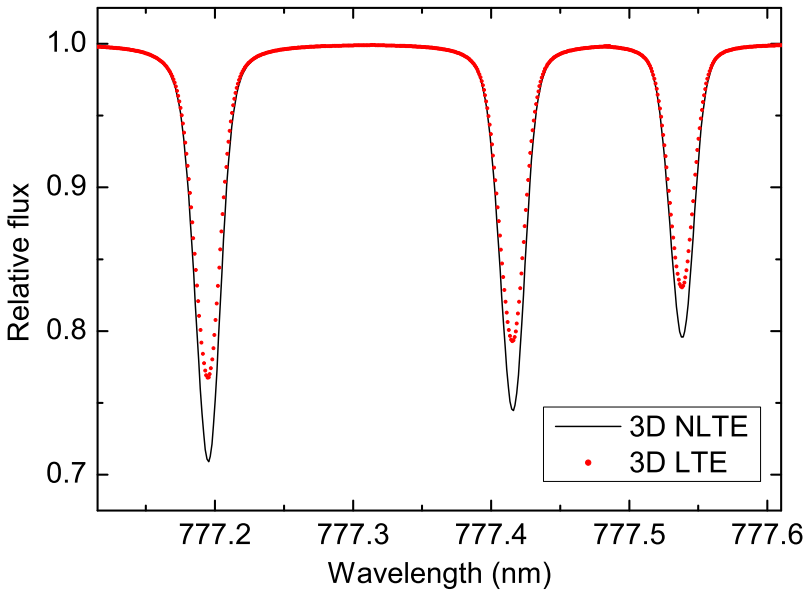

Fig. 2. Synthetic 3D NLTE (black line) and 3D LTE (red dots) O I IR triplet lines in the solar spectrum calculated with identical oxygen abundance (disk-integrated flux spectrum). Spectral line synthesis calculations were done using twenty 3D model snapshots of a solar model atmosphere computed with the CO^{5}BOLD code.

cate that, in NLTE, line strengths are enhanced at every position on the disk and NLTE effects are more pronounced in the intergranular regions (low continuum intensity). Kiselman (1993) suggested that this happens because in the intergranular regions the triplet lines form higher in the atmosphere where the departures from LTE are more severe.

The origin of the NLTE effects can be examined by comparing NLTE and LTE line source functions and line opacities (see, e.g., the analysis of Kiselman 1993). Fig. 4 shows the ratio of NLTE and LTE line source functions (top panel) and line opacities (bottom panel) for the 777.19 nm component of the O I IR triplet, as given by Equations (1) and (2). As was stated previously, the $3p^5P$ sublevels share identical departure coefficients, so the factor $b_{\rm low}/b_{\rm up}$ that enters the equations and hence the ratios $S_{\rm NLTE}/S_{\rm LTE}$ and $\kappa_{\rm NLTE}/\kappa_{\rm LTE}$ are identical for each component of the triplet.

The plot shows that the source function decreases below the local Planck function at $\log \tau_{\rm Ross} \lesssim 0.0$. Fig. 4 also contains two spatially and temporally averaged flux contribution functions for the line depression (see Magain 1986) that were computed at the line center (777.1954 nm) and wing (777.15 nm) of the line profile. It can be seen that the line wings form in a region where $S_{\rm NLTE}$ is identical or very similar to B_ν, while the line core forms where significant departures from LTE may occur.

On the other hand, the line opacity of the O I IR triplet stays close to LTE in the entire line forming region. The NLTE/LTE ratio of line opacities depends mostly on $b_{\rm low}$, which is close to unity in the entire optical depth range where the O I IR triplet lines form, while the sensitivity to $b_{\rm low}/b_{\rm up}$ ratio is rather small. Hence, the influence of NLTE effects on the line opacity is weak, and therefore it can be inferred that the strengthening of the O I IR

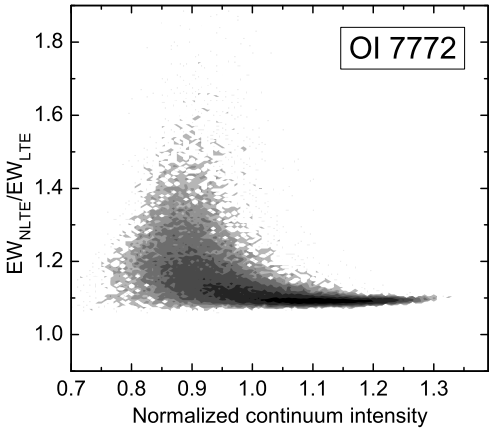

Fig. 3. Probability density plot showing the NLTE to LTE equivalent width ratio of the 777.19 nm component of the O I IR triplet, plotted against the normalized local continuum intensity for all twenty 3D model snapshots that were used in the calculations. Both continuum intensity and equivalent width refer to the disk-center solar spectrum (vertical rays).

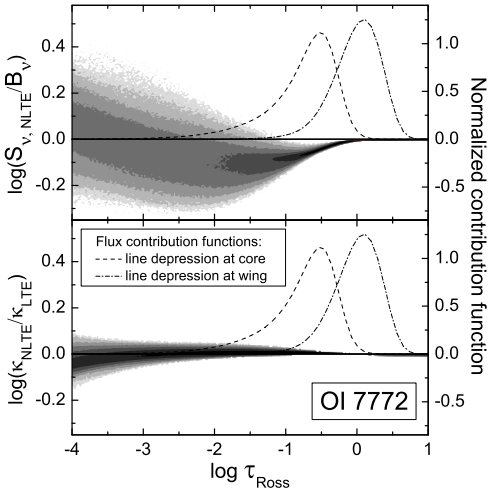

Fig. 4. NLTE-to-LTE ratio of the line source function (top panel) and line opacity (bottom panel) plotted versus Rosseland optical depth (gray scales represent the probability density). Both panels contain the same normalized flux contribution functions for the line depression at the core (777.1954 nm, dashed) and wing (777.15 nm, dot-dashed) of the O I 7772 line.

triplet happens solely due to the diminished line source function. According to Fabbian et al. (2009, and references therein), this is caused by the photon losses in the line.

3.2. Numerical issues

Fig. 5 shows the evolution of the equivalent width of the 777.19 nm line (top panel) and the relative change of EW (bottom panel) as a function of the iteration number. As stated previously, the Λ-iterations are continued until the relative change in all NLTE equivalent widths of the selected radiative transitions (green lines in Fig. 1) becomes less than 10^{-3} per iteration. Even though the triplet line shown in Fig. 5 satisfies the convergence criterion already after a small number of iterations, certain other lines (mainly the resonant UV lines, not shown in the figure) may show much slower convergence and may thus require significantly more iterations to obtain the final NLTE population densities.

The top panel of Fig. 5 shows that there is a wide range in the number of iterations required to arrive at the convergence limit: depending on the selected 3D model snapshot, it may be as low as ∼ 30 or as large as ∼ 500 (in the most extreme cases the EWs of O I IR triplet lines continue to grow even after ∼300 iterations). One should note, however, that the poor convergence properties of the ordinary Λ-iteration scheme pose a well-known problem in radiation transfer calculations. To quote Hubeny (2003): "it exhibits a pathological behavior in that the solution stabilizes (i.e. relative changes of the source function become extremely small) long before the correct solution is reached". All this indicates that a more efficient iteration scheme needs to be implemented into the NLTE3D code in order to make the computations more efficient and accurate.

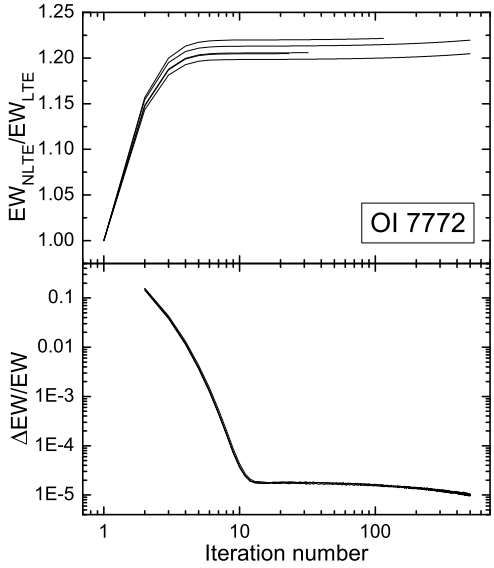

Fig. 5. Top panel: evolution of the disk-integrated equivalent width (EW) of the O I 777.159 nm line during the iteration process. Bottom panel: change per iteration in the EW of a given O I triplet component. The figure shows the iteration progress in five individual 3D model snapshots. Note that in the bottom panel data from the individual snapshots merge into one single curve.

4. Conclusions

We provide a short summary of our first results regarding the 3D NLTE spectrum synthesis of the O I IR triplet lines, carried out using a 3D hydrodynamical solar model atmosphere computed with the CO^{5}BOLD code. Atomic level population numbers were calculated using a significantly expanded and improved version of the NLTE3D code. Our results show that, in agreement with previous studies, the O I IR triplet lines are sensitive to NLTE effects, which lead to deeper line cores than those expected in LTE. This happens mainly because in the range of optical depths where the cores of the O I IR triplet lines form the line source function becomes smaller than the local Planck function. A significant deepening of the core, along with a net strengthening of the equivalent width of the line, leads to negative 3D NLTE–LTE abundance corrections.

The current version of the NLTE3D code utilizes an ordinary Λ-iteration scheme for the solution of non-linear statistical equilibrium equations. Such approach may be adequate in cases where all line transitions are weak and thus the radiative rates in the lines are only weakly coupled to the level populations (e.g. lithium). This, however, is obviously not true in the case of oxygen. For a proper treatment of this more general situation, the implementation of a faster and more reliable iteration scheme via some form of accelerated Λ-iteration (e.g. Olson et al. 1986; Rybicki & Hummer 1991) may be needed. This will be amongst the main priorities for the further development of the NLTE3D code, in order to ensure a higher reliability of the numerical results and a better versatility of the code in further applications involving more complicated model atoms.

Acknowledgements. This work was supported by grant from the Research Council of Lithuania MIP-101/2011. DP acknowledges financial support from Deutscher Akademischer Austausch Dienst (DAAD) that allowed exchange visits between Vilnius and Potsdam. MS acknowledges funding from the Research Council of Lithuania for a research visit to Vilnius. HGL, and EC acknowledge financial support by the Sonderforschungsbereich SFB 881 "The Milky Way System" (subproject A4) of the German Research Foundation (DFG).

References

Arnaud, M., & Rothenflug, R. 1985, A&AS, 60, 425
Asplund, M., Nordlund, Å., Trampedach, R., Allende Prieto, C., & Stein, R. F. 2000, A&A, 359, 729
Asplund, M., Grevesse, N., Sauval, A. J., Allende Prieto, C., & Kiselman, D. 2004, A&A, 417, 751
Barklem, P. S. 2007, A&A, 462, 781
Beeck, B., Collet, R., Steffen, M., et al. 2012, A&A, 539, A121
Böhm-Vitense, E. 1958, ZAp, 46, 108
Brott, I., & Hauschildt, P. H. 2005, The Three-Dimensional Universe with Gaia, 576, 565

Bruls, J. H. M. J., Rutten, R. J., & Shchukina, N. G. 1992, A&A, 265, 237
Caffau, E., Ludwig, H.-G., Steffen, M., et al. 2008, A&A, 488, 1031
Canuto, V. M., & Mazzitelli, I. 1991, ApJ, 370, 295
Castelli, F., & Kurucz, R. L. 2004, arXiv:astro-ph/0405087
Cayrel, R., Steffen, M., Chand, H., et al. 2007, A&A, 473, L37
Collet, R., Asplund, M., & Trampedach, R. 2007, A&A, 469, 687
Cunto, W., Mendoza, C., Ochsenbein, F., & Zeippen, C. J. 1993, A&A, 275, L5
Dobrovolskas, V., Kučinskas, A., Ludwig, H. G., et al. 2010, Proc. of 11th Symposium on Nuclei in the Cosmos, Proceedings of Science, ID 288
Dobrovolskas, V., Kučinskas, A., Steffen, M., Ludwig, H.-G., Prakapavičius, D., Klevas, J., Caffau, E., & Bonifacio, P. 2013, A&A, submitted
Drawin, H. W. 1969, Zeitschrift fur Physik, 225, 470
Fabbian, D., Asplund, M., Barklem, P. S., Carlsson, M., & Kiselman, D. 2009, A&A, 500, 1221
Freytag, B., Steffen, M., & Dorch, B. 2002, Astronomische Nachrichten, 323, 213
Freytag, B., Steffen, M., Ludwig, H.-G., et al. 2012, Journal of Computational Physics, 231, 919
Gustafsson, B., Edvardsson, B., Eriksson, K., et al. 2008, A&A, 486, 951
Hubeny, I. 2003, Stellar Atmosphere Modeling, 288, 17
Ivanauskas, A., Kučinskas, A., Ludwig, H. G., & Caffau, E. 2010, Proc. of 11th Symposium on Nuclei in the Cosmos, Proceedings of Science, ID 290
Lambert, D. L. 1993, Physica Scripta Volume T, 47, 186
Ludwig, H.-G., & Kučinskas, A. 2012, A&A, 547, A118
Kiselman, D. 1993, A&A, 275, 269
Kučinskas, A., Steffen, M., Ludwig, H.-G., et al. 2013, A&A, 549, A14
Magain, P. 1986, A&A, 163, 135
Mihalas, D. 1970, Series of Books in Astronomy and Astrophysics, San Francisco: Freeman, —c1970,
Nordlund, A. 1982, A&A, 107, 1
Olson, G. L., Auer, L. H., & Buchler, J. R. 1986, J. Quant. Spec. Radiat. Transf., 35, 431
Pereira, T. M. D., Asplund, M., & Kiselman, D. 2009, A&A, 508, 1403
Rybicki, G. B., & Hummer, D. G. 1991, A&A, 245, 171
Sbordone, L., Bonifacio, P., Caffau, E., et al. 2010, A&A, 522, A26
Seaton, M. J. 1962, Proceedings of the Physical Society, 79, 1105
Shchukina, N. G., Trujillo Bueno, J., & Asplund, M. 2005, ApJ, 618, 939
Steffen, M., Cayrel, R., Caffau, E., et al. 2012, Memorie della Societa Astronomica Italiana Supplementi, 22, 152
Stein, R. F., & Nordlund, A. 1998, ApJ, 499, 914
Thévenin, F., & Idiart, T. P. 1999, ApJ, 521, 753
Wedemeyer, S., Freytag, B., Steffen, M., Ludwig, H.-G., & Holweger, H. 2004, A&A, 414, 1121